Journal of Applied Physics

Robust magnetic domain of Pt/Co/Au/Cr_2O_3/Pt stacked films with a perpendicular exchange bias

Cite as: J. Appl. Phys. **127**, 153902 (2020); https://doi.org/10.1063/5.0002240
Submitted: 23 January 2020 • Accepted: 28 March 2020 • Published Online: 15 April 2020

Yu Shiratsuchi, Saori Yoshida, Hiroaki Yoshida, et al.

Journal of Applied Physics ARTICLE scitation.org/journal/jap

Robust magnetic domain of Pt/Co/Au/Cr_2O_3/Pt stacked films with a perpendicular exchange bias

Cite as: J. Appl. Phys. **127**, 153902 (2020); doi: 10.1063/5.0002240
Submitted: 23 January 2020 · Accepted: 28 March 2020 ·
Published Online: 15 April 2020

View Online Export Citation CrossMark

Yu Shiratsuchi,[1,a)] Saori Yoshida,[1] Hiroaki Yoshida,[1] Yoshinori Kotani,[2] Kentaro Toyoki,[1,2] Ryoichi Nakatani,[1] Chiharu Mitsumata,[3] and Tetsuya Nakamura[2]

AFFILIATIONS

[1]Department of Materials Science and Engineering, Graduate School of Engineering, Osaka University, 21-Yamadaoka, Suita, Osaka 565-0871, Japan
[2]Japan Synchrotron Radiation Research Institute (JASRI), 1-1-1 Kouto, Sayo, Hyogo 679-5198, Japan
[3]National Institute for Materials Science (NIMS), 1-2-1 Sengen, Tsukuba, Ibaraki 305-0047, Japan

[a)]**Author to whom correspondence should be addressed:** shiratsuchi@mat.eng.osaka-u.ac.jp

ABSTRACT

Magnetic domain pattern and magnetic domain wall motion are particularly important to understand the magnetization process. Here, we investigated the magnetization process of perpendicularly exchange-biased Pt/Co/Au/Cr_2O_3/Pt stacked films based on observations of the magnetic domain. In particular, in contrast to previous studies which use fully exchange-biased state, we used the bi-exchange-biased state. We found that the magnetic domain pattern at the remanent state was robust against magnetic-field cycling, which is relevant to the absence of the training effect. The magnetization process was followed by domain wall propagation in the increasing branch of the magnetization curve. In the decreasing branch, both nucleation of the reversed domain and domain wall propagation were involved. The former was accompanied by latency, suggesting that thermal activation played a significant role in the nucleation of the reversed domain.

INTRODUCTION

Magnetic domain pattern and magnetic domain wall motion are the key factors required to understand the magnetization process of magnetic materials. The magnetization process of general ferromagnets (FMs) is symmetric with respect to the applied magnetic-field direction. In contrast, in the case of the FM/antiferromagnet (AFM) stacked films, the magnetization process is often asymmetric because of the exchange bias (EB)[1–16] and/or the interfacial Dzyaloshinskii–Moriya interaction (DMI).[14,15] In the case of the exchange-biased system, the magnetization reversal mechanism of the FM layer is different for magnetic-field directions, i.e., in parallel and antiparallel to the EB direction. Although asymmetric magnetization reversal has been one of the most debated topics, understanding of the dominant mechanism of magnetization reversal is still insufficient, especially for perpendicular exchange-biased systems, with respect to the magnetic domain and domain wall motion. For some systems,[1,2,4] magnetization reversal is accompanied by nucleation and domain wall propagation in the ascending branch, i.e., the magnetic field is parallel to the EB direction, whereas either coherent rotation or propagation of a high density of reversed domain nucleation dominates in the descending branch. In the other system, the opposite behavior has been reported.[3,5]

In this study, we investigated the magnetization processes of a perpendicularly exchange-biased system, Pt/Co/Au/Cr_2O_3/Pt stacked films, based on magnetic domain observations. We employed the multi-domain state exhibiting double EB[17,18] as an initial state (hereafter, described as bi-EB state), which was defined by zero-field cooling (ZFC) after demagnetization at room temperature (see below). In our previous study, we observed the bi-EB state in Pt/Co/Au/Cr_2O_3/Pt stacked films[17] and found that EB polarity is coupled with the magnetic domain at the remanent state in a domain-by-domain basis.[20] The bi-EB state has been rarely used to investigate interfacial exchange coupling between FM and AFM domains,[18] whereas most previous studies have employed the magnetization process of the fully exchange-biased state, i.e., after field cooling (FC).[1–16] Although the bi-EB state was shown in our previous paper,[17,21] the magnetization process of the bi-exchange-biased ferromagnetic magnetization has not been investigated, which is the main focus of this paper. Owing to this approach, we can address

(1) the magnetization process in the low magnetic-field regime, i.e., an external field $H <$ EB field H_{EB} and (2) the robustness of the magnetic domain pattern at the remanent state for magnetic-field cycling, which is coupled with the training effect, both of which have been focused on in this study.

EXPERIMENTAL

Samples were fabricated using a DC magnetron sputtering system with a base pressure lower than 5×10^{-6} Pa. The stacked structure of the films was designed as follows: Pt(1.2, 1.5)/Co(0.4)/Au(0.5)/Cr_2O_3(200)/Pt(20). The films were prepared on an α-Al_2O_3(0001) single-crystalline substrate. The thickness of the Pt capping layer was chosen to obtain the suitable magnetic domain size by altering the saturation magnetization and the effective magnetic anisotropy energy. Numbers in parenthesis of each layer denote the thickness in nanometer units. A 20-nm thick Pt buffer layer was deposited at 873 K to fabricate the twinned (111) structure. On the Pt buffer layer, a Cr_2O_3(0001) layer was deposited at 773 K via reactive sputtering using a pure Cr target with $Ar + O_2$ gas mixture. The Au, Co, and Pt capping layers were deposited on the Cr_2O_3 layer at room temperature. More details of the fabrication processes and structural information of the film can be found in our previous study.[21]

Magnetic easy direction and saturation magnetization, M_S, were checked using the magnetization curves measured by vibrating sample magnetometry (VSM) and magneto-optic Kerr effect (MOKE) magnetometry with a polar configuration. Figure 1 shows the typical magnetization curves measured at room temperature. Note that the vertical axis of the VSM data (the left axis) denotes the magnetization per area, $M_S \cdot t_{FM}$, because the spin-polarization of Pt and Au attached

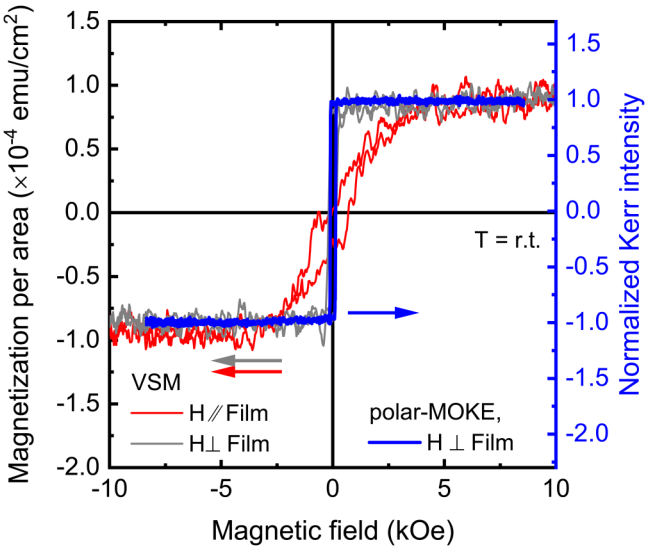

FIG. 1. Magnetization curves measured at room temperature. The gray and red curves denote measurements obtained by VSM, and the blue curve denotes measurements obtained by MOKE. Applied field was parallel (red) and perpendicular (gray and blue) to the film plane.

with Co contribute to the M_S. The $M_S{}^*t_{FM}$ is about 0.9×10^{-4} emu/cm, which is higher than our previous report,[21] which may be due to the difference of the Curie temperature of the ultrathin (0.4 nm) Co film. As can be clearly seen, the film showed perpendicular magnetic anisotropy. Based on this, the magnetic field in the following experiments was applied to the direction perpendicular to the film. Thus, perpendicular EB is studied here. Perpendicular EB is favored for the crystallographic orientation of the Cr_2O_3 layer, i.e., the (0001) growth, because Cr_2O_3 has uniaxial magnetic anisotropy with the easy axis parallel to the *c*-axis.[22]

We defined the bi-EB state in the following ways: (1) the film was demagnetized by the DC magnetic field around the coercivity, H_C, at room temperature (above the blocking temperature T_B) while directly observing the formation of the magnetic domain by a magneto-optic Kerr effect (MOKE) microscope. (2) The sample was cooled to the measurement temperature (below T_B) in maintaining the demagnetized state under the zero-magnetic field, i.e., the zero-field-cooling (ZFC). Note that T_B of the studied film was determined from the temperature dependence of the EB field after FC (not shown), i.e., the fully EB state, as 293 K, which is similar to the Néel temperature of a Cr_2O_3(0001) thin film determined by the spin Hall magnetoresistance (SMR) effect.[23] It should also be noted that the demagnetized magnetic domain state was stable during the ZFC process, which was confirmed by the MOKE microscope. For the magnetic domain observation, a suitable observation method had to be chosen depending on aspects such as the observation area, the required resolution, and the data acquisition time. We used two techniques: scanning soft x-ray magnetic circular dichroism (XMCD) microscopy[19,24] and MOKE microscopy. The magnetic domain patterns from the XMCD microscope were collected using the difference between the spatial distributions of the absorption intensity for fixed helicity, i.e., $(\mu_+ - \mu_-)/(\mu_+ + \mu_-)$ where μ_+ and μ_- are the absorption intensity for the positive and negative helicities, respectively. The acquisition time of one XMCD image was about 45 min, i.e., ~20 min for one image with fixed helicity and ~5 min for changing helicity. The resolution of the XMCD microscope was determined by the focused size of the soft x-ray and the pixel size, which were about 150 nm.[25] The photon energy of the incident soft x-ray was 778.5 eV, i.e., the Co L_3 edge. The experiments using the XMCD microscope were performed at the beamline BL25SU of SPring-8 synchrotron facility. Details regarding the XMCD microscope have been previously published.[24] In the MOKE microscope, the acquisition time of the data was determined by the exposure time and the frame rate of the CCD camera, which were set as 1/60 s. The imaging size, resolution, and data acquisition time per image for the two techniques are summarized in Table I. In this study, the magnetic-field dependence of the magnetic domain pattern after several magnetic-field cycles was measured. The scanning XMCD microscope was mainly used to obtain images of small magnetic domains that were difficult to resolve by the MOKE microscope. The MOKE microscope was mainly used to investigate the time-resolved magnetic domain pattern.

RESULTS AND DISCUSSIONS

Figure 2 shows the MOKE loop of the film with the 1.2-nm thick Pt capping layer measured at 265 K after ZFC with the

TABLE I. Image size, acquisition time, and resolution of the scanning XMCD microscope and MOKE microscope used in this study.

	Scanning XMCD microscope	MOKE microscope
Image size	$60 \times 60\,\mu m^2$	$107 \times 80\,\mu m^2$ (1280 × 860 pixel)
Acquisition time	Approximately 45 min for both helicities	1/60 s
(time resolution)	Approximately 20 min for one helicity	
Resolution	Approximately 150 nm[25]	Approximately a few μm

demagnetization. The loop comprised two loops shifted to the opposite magnetic-field direction. The shift of each loop, i.e., H_{EB}, was calculated to be ~700 Oe for the positive part and ~670 Oe for the negative part. H_{EB} is greater than the width of each loop, i.e., H_C, which is ~200 Oe; consequently, the MOKE loop is the double-shifted one. The deviation of the remanent value from zero is due to the imperfect demagnetization at room temperature. In an inset, the MOKE loops measured several times are shown. It is clear that the loop shape is identical, which indicates the absence of the training effect for both positive and negative EBs. The absence of the training effect can be explained by the symmetry of the magnetic anisotropy of Cr_2O_3. Because the magnetic anisotropy of Cr_2O_3 is uniaxial, both FM and AFM spins are directed perpendicular to the film. Hence, we can reasonably assume that FM and AFM spins are coupled with collinear spin alignment. The spin frustration in the AFM layer, which can cause relaxation of the magnetic domain state and consequently the training effect, does not accrue.[26] This is in contrast to the case when the multi-domain was formed by the magneto-electric field cooling (MEFC), where a significant training effect and a change in the magnetic domain pattern by the magnetic-field cycle were observed.[17] In the case of the MEFC, the magnetic inhomogeneity is caused by the energy competition between the interfacial exchange coupling and the ME-effect at the bulk site of the Cr_2O_3 layer, yielding the frustrated magnetic domain structure in the Cr_2O_3 layer.

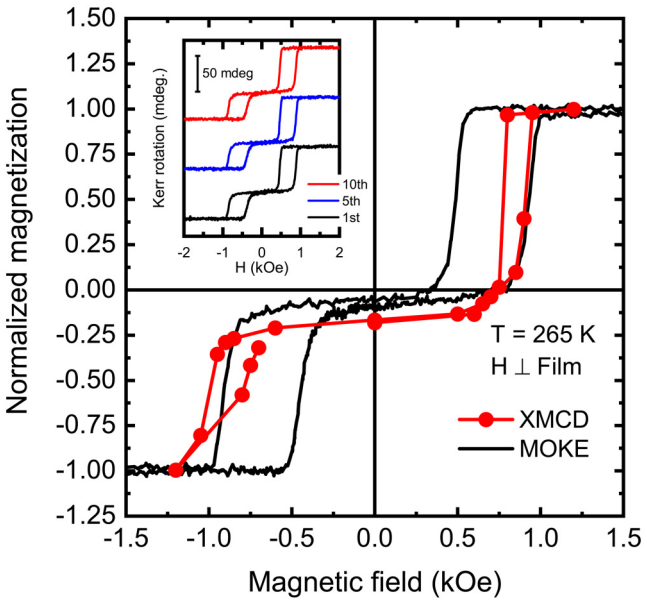

FIG. 2. MOKE loop measured at 265 K after ZFC while maintaining the demagnetized state. The film used was a Pt(1.2)/Co(0.4)/Au(1.0)/Cr_2O_3(200)/Pt(20) stacked film, identical to the film used for magnetic domain observation using the scanning XMCD microscope. The vertical axis was normalized by the saturated value. Inset shows the MOKE loops after ZFC measured with first (black), fifth (blue), and tenth (red) magnetic-field cycles showing the absence of the training effect. Loops are shifted in the vertical direction to see easily.

The double/skewed loop was observed for the demagnetized in-plane EB film, i.e., as-deposited, non-annealed film.[27] In such a case, it was likely to be difficult to regain the similar demagnetized state even with the demagnetizing at the elevated temperature. This is probably because the possible AFM spin orientation is in-plane random because of the poly-crystalline nature and the similar interfacial AFM spin alignment may be difficult to be reproduced. In contrast, our film has the perpendicular EB where the interfacial AFM (Cr) spin orientation can be restricted up or down owing to the (0001) orientation of the Cr_2O_3 layer.[21] In this case, the double EB state itself could be well reproduced by the above processes. Although the degree of the demagnetization, which manifests as the remanent magnetization, and the precise magnetic domain pattern are difficult to be reproduced perfectly, as long as the AFM domain state and the total magnetic energy including the interfacial exchange coupling are stable, the training effect can be absent.

Figure 3 shows the magnetic domain pattern at various magnetic fields. As shown in Fig. 3(a), the magnetic domain pattern is the multi-domain state at zero field, which agrees with the results of previous studies.[20] With increasing magnetic field, the magnetic domain with upward magnetization (blue domains) expands and the magnetic domain with downward magnetization (red domains) shrinks in maintaining the contour of each magnetic domain, which indicates that the magnetization process is dominated by the propagation of the static magnetic domain wall. After applying 1.2 kOe, which is higher than the saturation field of ~1.0 kOe (see Fig. 2), the magnetic field was reduced. At 800 Oe, some reversed magnetic domains (red domains) were nucleated. The nucleation may have easily occurred along the vertical line, which is probably the grain boundary. When the magnetic field further decreased, many red domains were formed. Finally, after the magnetic field was removed [Fig. 3(l)], i.e., at the remanent state, the initial magnetic domain pattern was recovered. In the negative magnetic field, the magnetization process was similar to that for the positive branch. The integrated XMCD intensity at each magnetic field, which corresponds to the magnetization, is plotted in Fig. 2 and is denoted by red circles. The evolution of the magnetic domain pattern with the magnetic

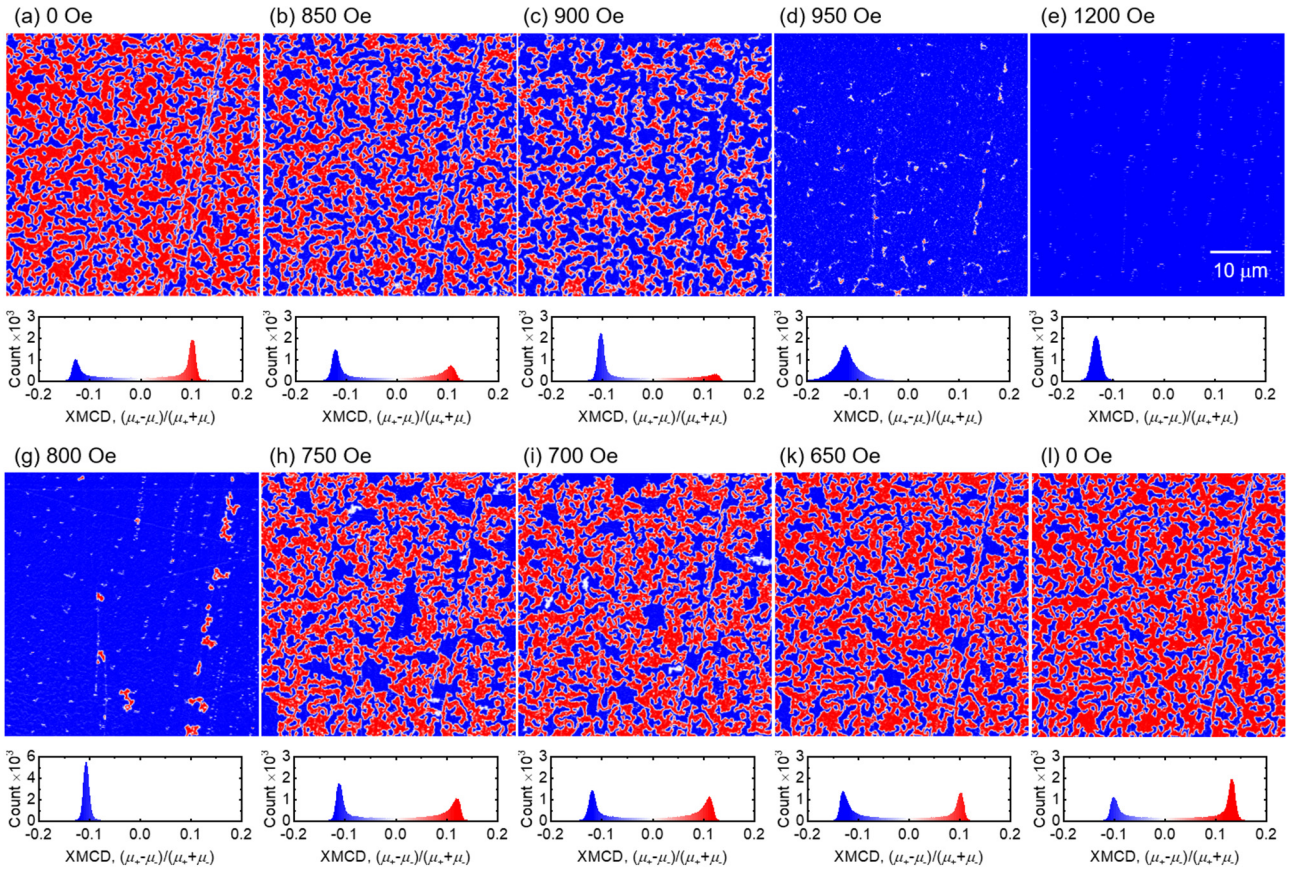

FIG. 3. Magnetic domain patterns and the corresponding histogram of XMCD intensity in [(a)–(e)] ascending and [(f)–(i)] descending branches of the magnetization curve observed using the scanning XMCD microscope. The film used was identical to the one used in Figs. 1 and 2. The blue and red domains correspond to the upward and downward magnetization directions, respectively. The positive direction of the magnetic field was defined as the upward direction.

field roughly matches the MOKE loop, which agrees with the results of our previous study, where the EB polarity was determined by the domain-by-domain basis.[20] The difference in the two loops is partly due to the difference in the magnetic field sweep rate, i.e., the data acquisition time for the two measurements: 60 s for the MOKE loop and ∼45 min for one data point of the XMCD. This effect manifests pronouncedly in the nucleation field because of the presence of the latency of the reversed magnetic domain nucleation (see below). The difference in the saturation field of the loop in the negative side is also seen, which implies the asymmetric domain wall motion with respect to the applied field direction.

We further investigated the robustness of the magnetic domain pattern at the remanent state because it is directly related to the training effect of EB. We applied the magnetic field below the saturation field, which expanded the blue domain by the partial displacement of the magnetic domain wall, as shown in Fig. 4(b). After the magnetic field was removed from Fig. 4(b), the magnetic domain pattern was again recovered to the initial state; Figs. 4(a) and 4(c) are very similar. In this case, the process of recovery was dominated by the back flow of the magnetic domain wall, called the spring-back effect. This is in contrast to the previous case shown in Fig. 3, where the process of recovery was dominated by the nucleation of the reversed domain. The robustness of the magnetic domain state was consistent with the absence of the training effect, shown in the inset of Fig. 2, and the reports after FC in this system.[26,28,29]

In Figs. 3(h) and 3(i), some white domains are observed, which are formed when the revered domain is newly nucleated during the second scan to collect the differential image (see the above experimental procedure). This is due to the presence of a long latency for nucleation of the reversed domain. Indeed, we observed that the reversed domain was newly nucleated scan-by-scan, and the time dependence of the XMCD intensity led to a decay time of approximately 4000 s (not shown), which indicates that the thermal activation on the reversed domain nucleation[30–32] significantly affects even in the long-time measurements. We address the latency of the reversed domain nucleation more in detail based on the time-resolved magnetic domain imaging using the MOKE microscope. For this investigation, we used the film with $t_{Pt} = 1.5$ nm, where a

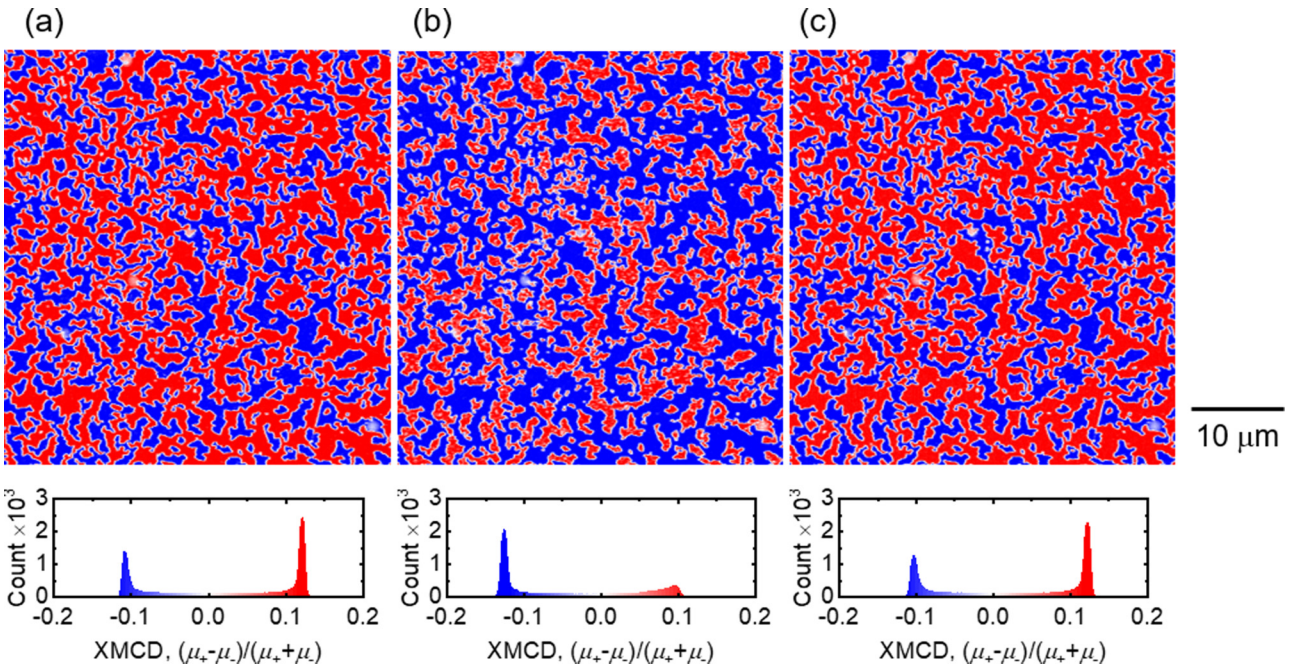

FIG. 4. Magnetic domain patterns and the corresponding histogram of XMCD intensity at (a) remanent and (b) partially magnetized states. (c) was collected after removing the magnetic field from (b). Definition of red and blue domains are same as those in Fig. 3.

large magnetic domain applicable to the MOKE microscope was observed. Similar to the XMCD measurements, the multi-domain state was formed by the DC magnetic field and was quenched to 278 K, which is lower than T_B. The magnetic-field sequence was as follows: the magnetic field was increased from 0 Oe (initial state) to +2000 Oe (above saturation field) and rapidly decreased to the keeping measurement field H_m. The time evolution of the magnetic domain pattern was recorded while maintaining the magnetic field at H_m. The time to stabilize the magnetic field at H_m from 2000 Oe was approximately 1–2 s, which was sufficiently short compared with the latency. Figure 5 shows the time evolution of the magnetic domain pattern observed at different positions on the same film. The reversed magnetic domain was suddenly nucleated with the latency of about 33/60 s. The nucleation occurred homogeneously within the time resolution of the instrument, which is 1/60 s, indicating that magnetic domain wall motion was not involved. We also found that the latency changed with every trial, which suggests that the nucleation of the reversed domain occurred stochastically because of thermal activation (see movies 1 and 2 in the supplementary material).

One may wonder whether we can rule out the magnetic domain wall propagation in the reversal process absolutely. To verify this, we performed similar measurements at another site on the same film, as shown in Fig. 5(b) (see also movie 3 in the supplementary material). After stabilizing the magnetic field to H_m, the small reversed magnetic domain (a few μm^2) was nucleated with a latency of 6/60 s. The magnetic domain wall propagated from this small nucleus. The propagation was not continuous but intermittent, indicating that thermal activation also affects domain wall pinning. Thus, the domain wall motion is in the creep regime. Note that the magnetic domain pattern at $t = 56/60$ s is not identical to the initial one because this is not a final state. Due to the instrumental limitation of the MOKE microscope, it is difficult to record the full recovering process. Even in this case, we confirmed that the magnetic domain pattern finally formed at the remanent state was identical to the initial one, i.e., a robust magnetic domain pattern was assured. The two types of the magnetization reversal shown in Fig. 5 occurred in the magnetic domains with the similar size. The different reversal mode in the similar sized magnetic domain is possibly due to the difference in the inhomogeneity of domain wall pinning energy and reversal field within the magnetic domain.

Based on the time-resolved observation of the magnetic domain, we can address the stochastic phenomena directly. Such an investigation will help understand the microscopic origin of EB in more detail through the quantitative evaluation of, for example, the activation volume and the energy barrier for magnetization reversal. We hope to investigate this in future. In addition, in this study, we focused on the EB, and the interfacial DMI was not considered. The stacking structure of our film, Pt/Co/Au/Cr_2O_3/Pt, was asymmetric, where finite interfacial DMI can be expected. The interfacial DMI could be pronounced by employing, for example, a Pt/Co/Cr_2O_3/Pt stacked system, which will be also investigated in the near future.

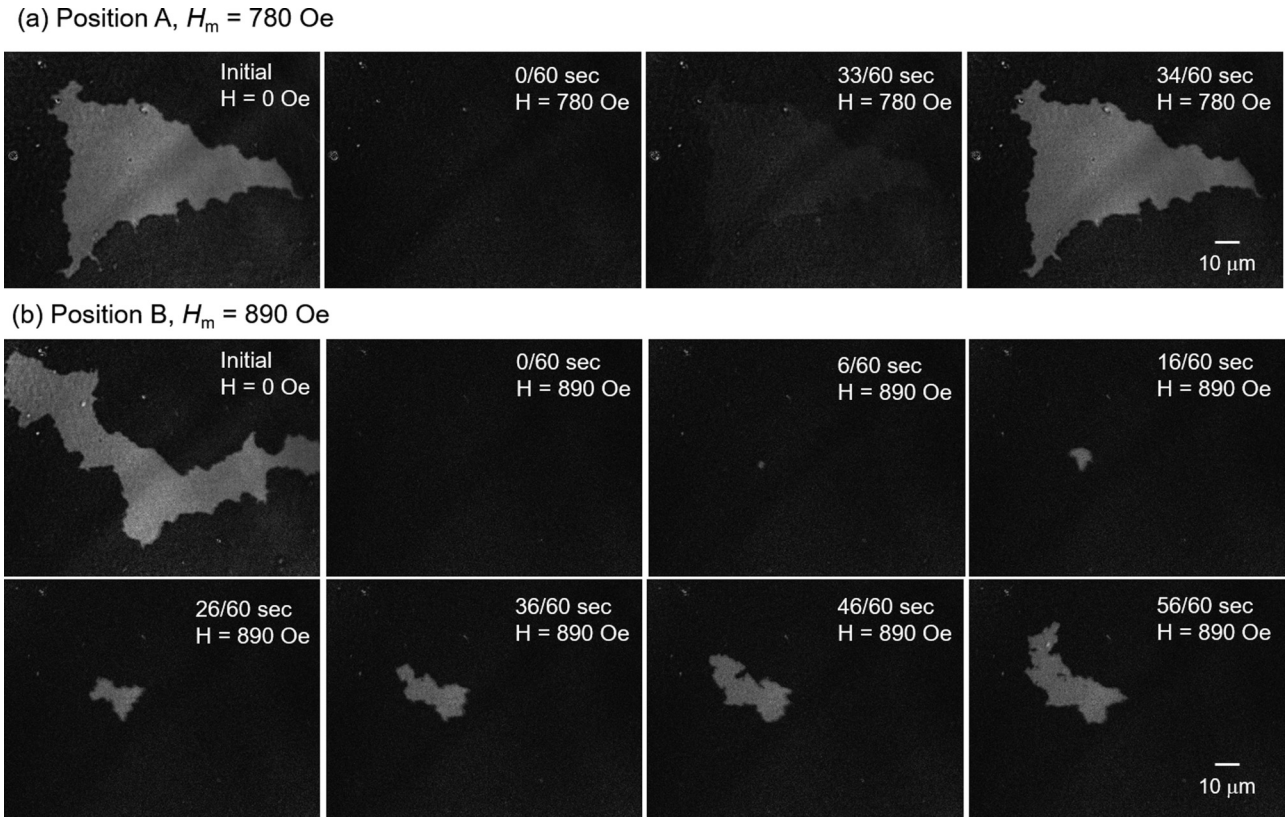

FIG. 5. Time dependence of magnetic domain pattern observed by the MOKE microscope. The measurement temperature was 278 K. Magnetic-field cycling was swept as 0 Oe → 1.3 kOe → H_m, and after cycling, the magnetic field was maintained at H_m during the magnetic domain observations. The frame rate and the exposure time of the CCD camera were both 1/60 s. (a) and (b) were collected on different areas of the same sample, and the H_m values for (a) and (b) were 780 Oe and 890 Oe, respectively.

SUMMARY

We investigated the magnetization process of a Pt/Co/Au/Cr_2O_3/Pt stacked film showing perpendicular EB. In particular, by employing the bi-EB state, we could address two aspects of the perpendicular EB system from a perspective of the direct observation of the magnetic domain state: (1) the magnetization process in the low field regime below H_{EB}, (2) the robustness of the magnetic domain state, which should couple with the training effect, and (3) the recovering process of the magnetic domain state with removing magnetic field. Consequently, we observed two types of magnetization processes—the magnetic domain wall propagation and the nucleation of the reversed magnetic domain—which were observed in increasing and decreasing magnetic fields, respectively. The magnetic domain pattern at the remanent state was robust for the magnetic-field cycle, which agrees with the absence of the training effect of EB. The magnetic domain pattern was recovered by the nucleation of the reversed domain or by the back flow of the magnetic domain wall. We found that nucleation of the reversed magnetic domain occurred with finite latency, which suggests that nucleation occurred stochastically by thermal activation.

SUPPLEMENTAL MATERIAL

See movies 1–3 in the supplementary material, which shows the magnetization reversal process with latency shown in Fig. 5. Movies 1 and 2 show the results for the two different trials for the same magnetic-field sequence shown in Fig. 5(a).

ACKNOWLEDGMENTS

Magnetic domain observations using the scanning XMCD microscope were carried out with the approval of the JASRI (Proposal Nos. 2015B0079 and 2016A0079). This work was partly supported by the JSPS KAKENHI (Grant Nos. 16H03832, 16H02389, and 19H00825). The scanning XMCD microscope was developed with the support by the Elements Strategy Initiative Center for Magnetic Materials (ESICMM) (Grant No. 12016013), through the Ministry of Education, Culture, Sports, Science and Technology (MEXT).

REFERENCES

[1]M. R. Fitzsimmons, P. Yashar, C. Leighton, I. K. Schuller, J. Nogués, C. F. Majkrzak, and J. A. Dura, Phys. Rev. Lett. **84**, 3986 (2000).

[2]A. Kirilyuk, T. Rasing, H. Jaffrés, D. Lacour, and F. Nguyen Van Dau, J. Appl. Phys. **91**, 7745 (2002).
[3]J. McCord, Schäfer, R. Mattheis, and K.-U. Barholz, J. Appl. Phys. **93**, 5491 (2003).
[4]F. Romanens, S. Pizzini, F. Yokaichiya, M. Bonfim, Y. Pennec, J. Camarero, J. Vogel, J. Sort, F. Garcia, B. Rodmacq, and B. Dieny, Phys. Rev. B **72**, 134410 (2005).
[5]P. Blomqvist, K. M. Krishnan, and H. Ohldag, Phys. Rev. Lett. **94**, 107203 (2005).
[6]J. Camarero, J. Sort, A. Hoffmann, J. M. García-Martín, B. Dieny, R. Miranda, and J. Nogués, Phys. Rev. Lett. **95**, 057204 (2005).
[7]G. Malinowsli, S. van Dijken, M. Czapkiewicz, and T. Stobiecki, Appl. Phys. Lett. **90**, 082501 (2007).
[8]M. Czapkiewicz, T. Stobiecki, and S. van Dijken, Phys. Rev. B **77**, 024416 (2008).
[9]S. Y. Suck, V. Neu, U. Wolff, S. Bahr, O. Bourgeois, and D. Givord, Appl. Phys. Lett. **95**, 162503 (2009).
[10]J. McCord and R. Schäfer, New J. Phys. **11**, 083016 (2009).
[11]H.-S. Lee, K.-S. Ryu, C.-Y. You, K.-R. Jeon, S.-H. Yang, S. S. P. Parkin, and S.-C. Shin, J. Appl. Phys. **111**, 07D731 (2012).
[12]Q. Wu, W. He, H.-L. Liu, Y.-F. Liu, J.-W. Cai, and Z.-H. Cheng, J. Appl. Phys. **113**, 033901 (2013).
[13]A. Fassatoui, R. Belhi, J. Vogel, S. Pizzini, P. David, and K. Abdelmoula, J. Magn. Magn. Mater. **449**, 475 (2018).
[14]R. A. Khan, H. T. Nembach, M. Ali, J. M. Shaw, C. H. Marrows, and T. A. Moore, Phys. Rev. B **98**, 064413 (2018).
[15]P. Kuświk, M. Matczak, M. Kowacz, K. Szuba-Jabłoński, N. Michalak, B. Szymański, A. Ehresmann, and F. Stobiecki, Phys. Rev. B **97**, 024404 (2018).
[16]Z. Shi, H. Zhong, W. J. Fan, S. M. Zhou, and J. Yuan, J. Magn. Magn. Mater. **474**, 127 (2019).
[17]Y. Shiratsuchi, S. Watanabe, S. Yonemura, T. Shibata, and R. Nakatani, AIP Adv. **8**, 125313 (2018).
[18]J. Jia, Y. Chen, B. Wang, B. Han, Y. Wu, Y. Wang, and J. Cao, J. Phys. D Appl. Phys. **52**, 065001 (2019).
[19]Y. Shiratsuchi, Y. Kotani, S. Yoshida, Y. Yoshikawa, K. Toyoki, A. Kobane, R. Nakatani, and T. Nakamura, AIMS Mater. Sci. **2**, 484 (2015).
[20]Y. Shiratsuchi, S. Watanabe, H. Yoshida, N. Kishida, R. Nakatani, Y. Kotani, K. Toyoki, and T. Nakamura, Appl. Phys. Lett. **113**, 242404 (2018).
[21]Y. Shiratsuchi, W. Kuroda, T. V. A. Nguyen, Y. Kotani, K. Toyoki, T. Nakamura, M. Suzuki, K. Nakamura, and R. Nakatani, J. Appl. Phys. **121**, 073902 (2017).
[22]L. M. Corliss, J. M. Hastings, R. Nathans, and G. Shirane, J. Appl. Phys. **36**, 1099 (1965).
[23]T. Iino, T. Moriyama, H. Iwaki, H. Aono, Y. Shiratsuchi, and T. Ono, Appl. Phys. Lett. **114**, 022402 (2019).
[24]Y. Kotani, Y. Senba, K. Toyoki, D. Billington, H. Okazaki, A. Yasui, W. Ueno, H. Ohashi, S. Hirosawa, Y. Shiratsuchi, and T. Nakamura, J. Synchrotron Radiat. **25**, 1444 (2018).
[25]Focused soft x-ray size was calculated one using the formula (Ref. 23) with the beamline specification and the adopted energy resolution, $E/\Delta E = 3000$.
[26]A. Hoffmann, Phys. Rev. Lett. **93**, 097203 (2004).
[27]R. Carpenter, G. Vallejo-Fernandez, and K. O'Grady, J. Appl. Phys. **115**, 17D715 (2014).
[28]K. D. Belashchenko, Phys. Rev. Lett. **105**, 147204 (2010).
[29]K. Toyoki, Y. Shiratsuchi, T. Nakamura, C. Mitsumata, S. Harimoto, Y. Takechi, T. Nishimura, H. Nomura, and R. Nakatani, Appl. Phys. Express **7**, 114201 (2014).
[30]E. Fulcomer and S. H. Charap, J. Appl. Phys. **43**, 4190 (1972).
[31]K. O'Grady, L. E. Fernandez-Outon, and G. Vallejo-Fernandez, J. Magn. Magn. Mater. **322**, 883 (2010).
[32]V. Baltz, B. Rodmacq, A. Zarefy, L. Lechevallier, and B. Dieny, Phys. Rev. B **81**, 052404 (2010).